Study on the effect of curvature on the aerodynamic properties of drone rotor blades

Riccardo Cagnato
riccardo.cagnato.1@gmail.com
Instituto Superior Técnico, Universidade de Lisboa, Portugal
June 2020

Abstract

The present work aims to study the effect of a curved leading edge in drone rotors blades, to see whether it can bring performance improvements. Ten different rotors are studied, having different blade geometries: the straight blade, the single curved blade, and two totally curved blades, having different tip shapes. The curvature is inserted both in forward and backward direction. At first, a Matlab code implementing the Blade Element Theory and the Blade Element and Momentum Theory has been realized. With this tool, it is possible to make comparison between different rotors, changing various geometrical parameters. The obtained results showed good agreement in the analysis of full-scale rotors. The need of taking into consideration 3D and low Reynolds number effects in the aerodynamic parameters led to the development of CFD simulations. The Moving Reference Method is chosen for the simulations, and a sensitivity study on how various parameters affect results is made. Then, the performances of the rotors while producing different amounts of thrust are studied, at first in hovering condition, and then in ascending flight conditions. The straight blade appears to be the best configuration for most of the cases, even though there are some conditions in which the total curved blade with the tip shape TE2 behaves better. This study also shows that in hovering the backward curved blades operate better than the forward curved blades, so a preference in the curvature direction is found. In order to isolate the curvature effect, a tip standardization is inserted an analyzed. Different 3D printing methods have been tested to produce the rotors, and SLA-printed rotors have been experimentally tested to study the hovering performances, verifying the similarity with the computational results.

1. Introduction

The drone sector is exponentially expanding, and there are reasons to believe that drones will be present more and more in everyday life. Their use in the military field is established, since they can access remote zones and scan them with high-tech cameras, as well as transport first aid kits. Delivering systems and public transportation are thought to be the next areas which will be covered by their use. The company Amazon launched the project Prime Air, to use drones for fast deliveries, realizing the first flight test in 2016, while the delivery company AHA started a partnership with Flytrex in 2017 to expand the delivery network in the Iceland capital Reykjavik. In Switzerland drones started to connect laboratories and the EOC hospital group, transporting laboratory samples and extra blood bags. Studies were made to understand whether the use of drones in the transportation field can be convenient with respect to the classical use of trucks [1], [2]. Another sector that is foreseen to live a great development in the next years is the Electric-Vertical-Take-Off-and-Landing-aircraft (EVTOL), in which both startups and companies are investing. Among the startups, the german Volocopter produced the Volocopter 2X model, capable of transporting two people by means of 18 small rotors driven by lithium-ion batteries [3]. Airbus flight-tested the one-seater model Vahana and the four-seater City Airbus to verify the feasibility of this new technology [4]. For all these applications, increasing the small-scale rotors aerodynamic performances appears fundamental. In fact, the low Reynolds number regime in which they operate results in a decrease of the aerodynamic efficiency, as found in many experimental studies [5] [6]. The formation of a laminar separation bubble is addressed as the cause for this behavior. This bubble is generated when a laminar boundary layer encounters an adverse pressure gradient which causes its separation. After the separation, the flow becomes turbulent and it recirculates. Its characteristics strongly depend on the angle of attack, the profile type, and the surface quality. Ohtake & others [7] experimentally found a strong non-linearity for the NACA 0012 lift coefficient at low Re and at low angles of attack, with the possibility of generation of a negative lift force (see figure 1.1). Their results were also confirmed by the computational work in [8], [9].

To understand how different rotor parameters affect

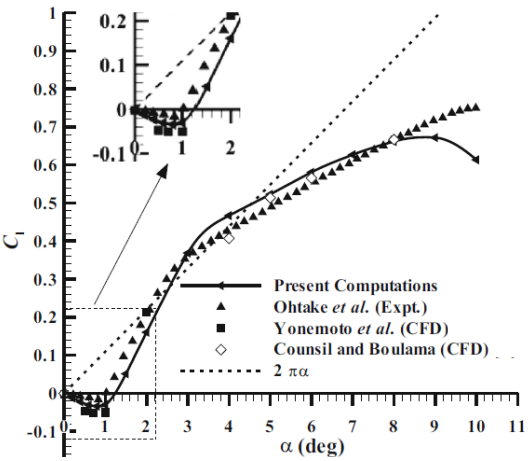

Figure 1.1: Non-linear behavior for the lift coefficient of NACA 0012 airfoil at Re=50,000. From [8]

performances, Ramasamy [10] studied how twisting rate and airfoil shape affect rotor thrust and power, and he used the Particle Image Velocimetry technique (PIV) to understand how the wake region is influenced by these geometric parameters. In this way, he discovered that the vortex sheets at low Reynolds are much thicker and turbulent with respect to normal scale rotors, occupying a substantial part of the wake.

Benedict & others [11] experimentally studied the fact of changing airfoil shape, twisting rate, tapering, blades number, and the presence of tip winglets, arriving to the definition of an optimum hovering rotor. This rotor is characterized by a very thin cambered airfoil, a long chord, and the presence of tapering. The tip winglets appeared to be very important in reducing the tip vortices. However, the effect of a curved leading edge was not considered, and this justifies the aim of the present work.

Computational Fluid Dynamics (CFD) appears as a powerful tool for this purpose, since its accuracy increased in the last years, together with the decreasing of the computational time. Two of the main methods for studying the flowfield around rotating objects are the Moving Reference Frame method (MRF), and the Moving Mesh method. The first treats the problem as steady, and needs the computational domain to be divided in a fixed part and moving part(s): the equations inside the moving domain are solved in a reference frame that is rotating with the angular velocity of the object studied, to simulate the rotation. In the second method, the entire mesh of the moving domain is put in rotation, so that unsteady phenomena can be taken into account. The work of Kutty & Rajendran [12] showed a good accordance between simulation and experimental results for APC propellers at different advance speeds, thus approving the MRF method for propeller performance analysis. Stajuda, Karczewski & others [13] found out that the domain dimensions strongly influence the results, and should be calibrated with experimental data once fixed the rotational speed, to increase the accuracy.

Rapid prototyping procedures lead to fast and accurate production of samples, and their use is foreseen to increase strongly in the next period. The last part of this work deals with testing different 3D printing procedures to see whether they can be applied to produce small-scale rotors. In particular, the Fused Deposition Modeling (FDM) and the Stereolithography (SLA) techniques are investigated. The rotors printed are tested in a University test bench to verify the CFD simulations, and to have a better insight on the performances.

2. Background

2.1. Momentum Theory

The Momentum theory describes the performance of rotating blades by means of a monodimensional and steady approach. Under the hypotheses of incompressible fluid, quasi-stationary regime and constant fluid properties in planes parallels to the rotor disk, the conservation laws are solved for a control volume which surrounds the rotor. The thrust produced by a rotor can be expressed as the product between the mass flow passing through the rotor disk $\dot{m}$ and twice the induced velocity v_i, that represents how the rotor movement is increasing the flow velocity.

$$T = 2\dot{m}v_i \qquad (2.1)$$

The induced ideal power requirement, not considering the viscous drag, is expressed as:

$$P_i = Tv_i \qquad (2.2)$$

An important performance parameter which comes from this theory is the Figure of Merit (FM), expressed as the ratio between the ideal and the actual power requirements in hovering condition:

$$FM = \frac{P_i}{P_{real}} \qquad (2.3)$$

In which P_{real} take into account also the viscous losses. Through this parameter, rotors having the same disk area can be confronted. The Momentum theory can be extended also to the case of axial and forward flight, see [14] for reference.

2.2. Blade Element Theory & Blade Element and Momentum Theory

The Blade Element Theory (BET) is a common way to approach the preliminary design of a rotor, permitting the determination of aerodynamic loads at predefined stations, and obtaining the overall values by integration along the blade. It is based on the principle that successive blade elements are independent, and this fact, while being acceptable for helicopter scale rotors, could cause inaccuracies when analyzing small

scale rotors. Linking the BET with the Momentum theory, an iterative determination of the induced velocity field along the blade is possible, this approach named Blade Element and Momentum Theory (BEMT). With the procedure described in [14], the following expressions for induced velocity λ, thrust coefficient dC_T and power coefficient dC_P at each blade element can be defined:

$$\lambda(r,\theta) = -\left(\frac{\sigma c_{l\alpha}}{16F}\right) + \sqrt{\left(\frac{\sigma c_{l\alpha}}{16F}\right)^2 + \frac{\sigma c_{l\alpha}\theta r}{8F}} \quad (2.4)$$

$$dC_T = \frac{1}{2}\sigma r^2 (c_L cos\phi - c_D \sin\phi) dr \quad (2.5)$$

$$dC_P = \frac{1}{2}\sigma r^3 (c_L \sin\phi + c_D \cos\phi) dr \quad (2.6)$$

In equation 2.4, the parameter F is the Prandtl tip loss factor, which is needed to model the loss of thrust production towards the blade tip. The integration along the blade of expressions 2.5-2.6 give the total amount of thrust produced and power required. Once obtained these values, the FM calculation is straightforward:

$$FM = \frac{C_T^{1.5}}{\sqrt{2}C_P} \quad (2.7)$$

The axial and forward flight modeling through BEMT is described in [14].

3. Matlab implementation of BET and BEMT

The BEMT theory is implemented in two Matlab programs which have different aims. The first program presents as input a thrust coefficient to be reached, and the blade planform: the root pitch angle is changed until the desired thrust production is reached. The second program evaluates the rotor performances having as input the complete rotor geometry, as well as the flight conditions. The blade curvature is inserted by means of a union of two circumferences which define the spatial development of the blade mean line. Changing the circumferences radiuses gives the possibility of changing the curvature typology.

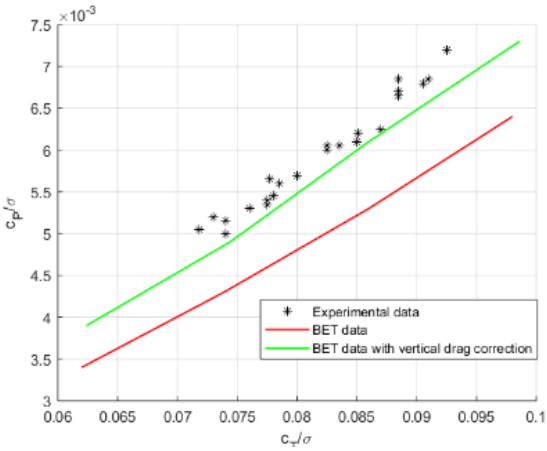

Figure 3.1: Comparison between experimental data and theorical data for the Wessex helicopter in hover condition

The lift and drag coefficients c_L and c_D for different discrete angles of attack α are determined with the program XFOIL [15]. In this way, it is possible to define the Re regime, as well as the intervals of angles of attack to be considered. The Matlab function *polyfit* is then used to create the interpolant polynomials, so that the c_L and c_D values can be extrapolated at every blade element, once α is known. In case of hovering flight condition, the first method has been verified through a comparison with the data of the Wessex helicopter, presented in [16]. With the insertion of the vertical drag contribute, the theorical results fit better what experimentally found (see figure 3.1).

The results for the forward flight are compared with

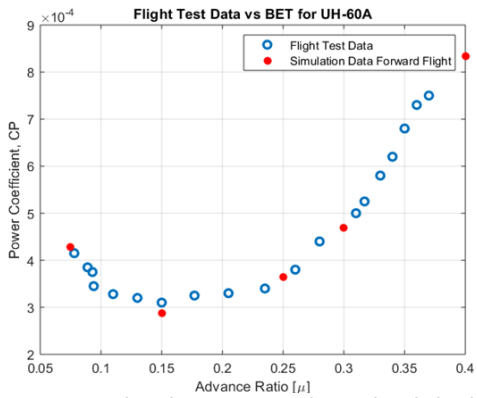

Figure 3.2: Comparison between experimental and simulation data for UH-60A main rotor

the main rotor of the Sikorsky UH-60A Black Hawk helicopter [17], simplifying its blades by considering only the SC1095 airfoil (see figure 3.2). The results showed a good agreement with flight test data, thus justifying the validity of the program for normal scale rotors.

Considering small scale propellers, the operative Re regime causes a decrease in the aerodynamic efficiency, and a strong nonlinearity in the lift polar. This fact affects the results obtained with the BEMT in the case of small-scale rotors, since the assumption of a linear relation between c_L and α cannot be ensured. Moreover, trying to linearize this behavior with different lift slopes would cause different induced velocity distributions, thus influencing the performance calculation. Figure 3.3

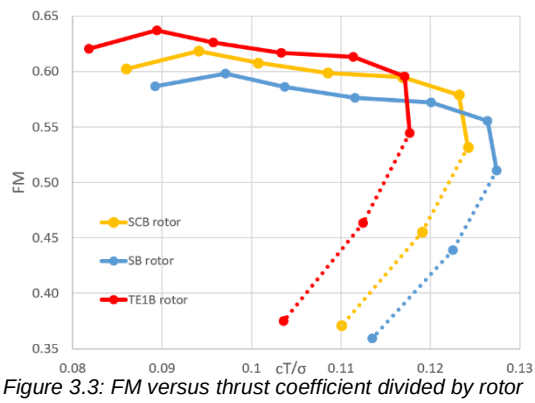

Figure 3.3: FM versus thrust coefficient divided by rotor solidity σ, obtained with the Matlab implementation of BEMT

shows the BEMT results for the analysis of subscale rotors. In table 1 it is possible to see the geometry of the rotors tested. The dashed lines represent rotors with a high pitch angle, for which the results are a lower thrust production due to a decrease in the lift production of NACA 0012 at low Re numbers. From this analysis it seems that the insertion of a curved leading edge may cause a benefit for the hovering performances. However, a deeper verification must be done, thus leading to the development of CFD simulations.

4. CFD simulations

For the computational study of the flow behavior around small scale propellers, the MRF method is chosen. In fact, the literature study showed how this method can produce reliable results in predicting rotors performance, especially adapting the proper moving domain dimension through comparison with experimental data [13]. The MRF is based on the fluid domain division in two parts, one that enclosures the rotor, the *moving zone*, and the rest of the domain, the *fixed zone*. In the moving domain the Navier-Stokes equations are solved with respect to a frame that is rotating with the angular velocity of the rotor, while in the fixed domain the equations are solved in the usual reference frame. The determination of the equations which characterize this method is presented in [18]. The turbulence model used for the simulations is the $\boldsymbol{k-\omega\ SST}$, because of its ability of automatically manage the transition between viscous sublayer and logarithmic layer in the boundary layer region. In the case of hovering flight, the boundary conditions are a pressure inlet and a pressure outlet equal to the atmospheric pressure, while the outer wall of the rotating domain is treated as a stationary wall. The rotor is addressed as a moving wall, with no relative velocity with respect to the moving domain, as suggested in [18]. When considering the case of axial flight, the only change made in the boundary condition is the velocity inlet, inserting the ascensional velocity.

4.1. Rotor geometrical model

The NACA 0012 is the airfoil chosen for the blades, having a chord equal to 20 mm. The trailing edge presents a width of 0.3 mm in order to improve the mesh quality in that region, and the hub is modeled as a cylinder having an external radius of 15 mm, and an internal hole of 5mm diameter. The radial dimension for each blade is kept equal to 120.44 mm. Ten blade planforms are modeled and resumed in table 1. For the single curved blade, the curvature starts at 70% of the radius and follows a circumference of 57.15 mm to reach the required radial dimension R of 120.44 mm. The total curved blades shape is modeled through a path defined by two circumferences of radiuses

Table 1: Rotor prototypes and nomenclature

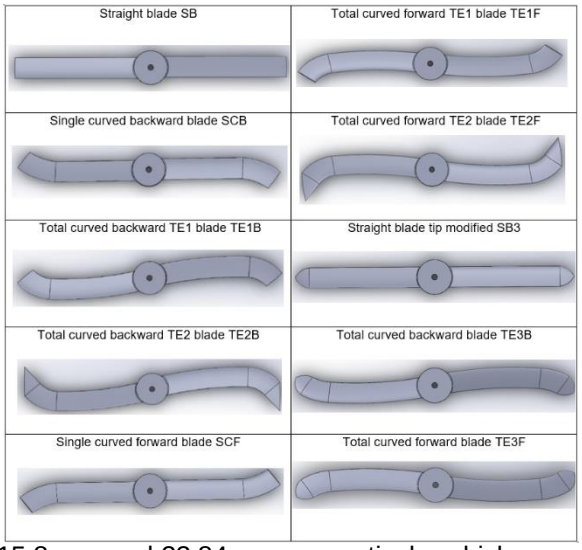

315.8 mm and 33.84 mm respectively, which merge in a point located at 75% of the blade radius, and $0.1R$ above the airfoil mean point. The TE1 tip follows the curvature of the blade mean-line while staying perpendicular to it, while TE2 tip presents an additive part to ensure that the final blade section is parallel to the airflow. Finally, the last three rotors SB3, TE3B and TE3F present the same tip shape, defined by two arcs having 15 mm radius. In this way, the aim is to reduce the tip effect in order to focus on the curvature effect.

4.2. Domain definition, meshing procedure and setup

The overall computational domain is a cylinder of 7.06 m height and 3.54 m diameter. These dimensions permitted to put the outer boundaries far from the rotor to avoid any kind of interference. In section 4.3 the results of how different moving domain dimensions affect results are presented. Regarding the mesh, the unstructured type is chosen, with tetrahedral elements in most of the domain, and 5 layers of prisms near the rotor walls, to accurately describe the boundary layer. The first prism layer dimension is chosen keeping in mind the aim of using the wall function approach and aiming to keep $30 < y^+ < 300$. y^+ is a parameter which represents the relative importance between Reynolds and viscous stresses.
The coupled solver is used, which rewrites the mass & momentum equations in a coupled manner in order to solve them simultaneously, and the Full Multigrid initialization (Fmg) is used for initializing the solution. To enhance the quality of the results, a second order upwind discretization scheme is chosen [19].

4.3. Analysis of moving domain dimensions

The SB rotor with a 15° root pitch angle is chosen for the study of the moving domain dimensions, with an angular velocity of 3000 Rotations Per Minute (RPM). The rotor is located 2.25 m from the inlet surface, and the moving domain dimension is defined by three distances: {radial distance from the

rotor; distance above the rotor; distance below the rotor}.

While the moving domain increases, the overall computational domain is kept fixed to the values defined in section 4.2. Five moving domains are tested:

- Domain 1: {25 mm; 50 mm; 50 mm}
- Domain 2: {50 mm; 100 mm; 100 mm}
- Domain 3: {100 mm; 200 mm; 250 mm}
- Domain 4: {150 mm; 250 mm; 300 mm}
- Domain 5: {200 mm; 300 mm; 400 mm}

Changing the moving domain dimensions resulted in a variation of thrust, power, and consequently FM. There is no evidence of linear correlation between the domain size and thrust, as depicted in figure 4.1.

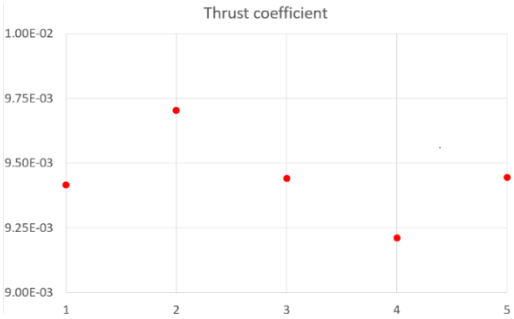

Figure 4.1: Thrust coefficient variation with different moving domains.

The domain 4 presented the lowest values in term of thrust, power and FM, so it is chosen as reference. The percentual differences relative to it are always less than 5.4% in term of thrust, 2.35% in term of power, and 6.2% in term of FM (table 2).

Table 2: Percentual discrepancies between different moving domains

	% Thrust	% Power	% FM
Domain 1	2.22%	1.17%	2.15%
Domain 2	5.35%	1.78%	6.24%
Domain 3	2.48%	0.96%	2.76%
Domain 4	0.00%	0.00%	0.00%
Domain 5	2.53%	2.35%	1.44%

From the analysis of the absolute velocity contours it is noticeable how the smaller domains are inadequate because the interface location is too near the rotor, thus hindering the flow development, causing a noticeable discontinuity (figure 4.2). In absence of experimental results, domain 4 is chosen as the basis for the simulations in this work, because of the good representation of the wake region together with the lower values of FM: in this way it is chosen to work in a lower quality estimate condition.

4.4. Analysis of mesh sensitivity

Four different meshes are tested, with increasing number of elements from a minimum of 1.29E6 to a maximum of 2.53E6. As the number of elements

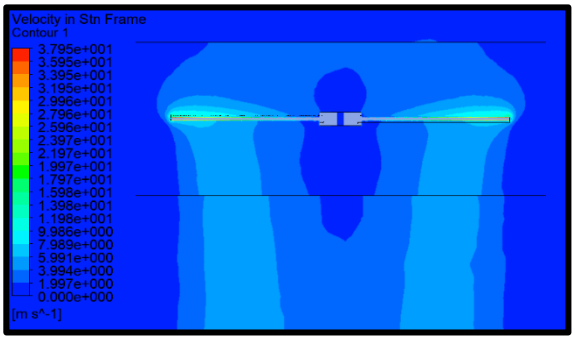

Figure 4.2: Velocity contour for domain 1. Notice the discontinuity near the interface region

is increased, the thrust gets higher (see figure 4.3), while an oscillation characterizes the power consumption. This causes the FM to increase, reaching an almost flat behavior between the medium fine and fine meshes.

Setting the finer mesh results as a reference, the percentual differences from them are evaluated, to understand the discrepancy, see table 3. The medium fine mesh is used for all the calculation in the present work.

Table 3: Discrepancies between results with different meshes

	ΔThrust	ΔPower	Δ FM
Coarse	4.48%	1.66%	8.16%
Medium	1.64%	1.35%	1.12%
Medium-fine	0.07%	1.75%	1.62%
Fine	-	-	-

5. CFD results

5.1. Rotational velocity variation

The SB rotor with a 15° pitch angle is used to test how a change in rotational speed between 2800 RPM and 6500 RPM affects the rotor performance. Eleven simulations are realized following an increasing speed order, to reach a faster convergence. The simulations demonstrate as expected that the thrust increase with the square of the angular speed while the power increases with the cube. The thrust and power coefficients present a reduced variation, of around 5% between 3000 RPM and 6500 RPM, and the FM gets higher when the rotor is rotating at higher angular velocities, varying between 0.42 and 0.45 for a global improvement of 9.2% between 3100 and 6500 RPM.

5.2. Untwisted blades-backward curvature

The first comparison is made between the rotors SB, SCB, TE1, TE2 with untwisted blades. The rotational speed is set constant and equal to 3000 RPM, while five root pitch angles are studied, namely 15°, 17°, 19°, 21°, 25° to increase the thrust production.

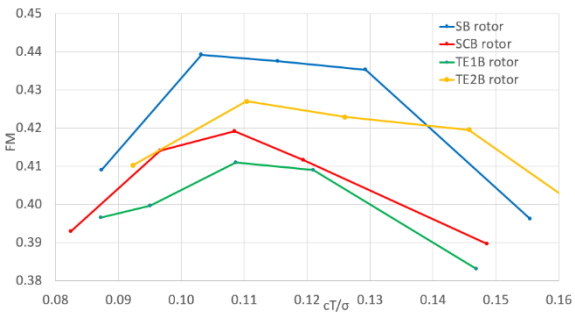

Figure 5.1: FM behavior for untwisted blades rotors, in case of backward curvature

The SB appears to be the best configuration for a great interval of normalized thrust coefficient $\frac{c_T}{\sigma}$, as can be seen in figure 5.1. With respect to SB, the SCB rotor produces less thrust while requiring more power to hover, so that a decrease in the overall performance is noticed. The different tip shape of TE1B and TE2B rotors causes TE2B to produce a higher thrust amount, between 5% and 20%, and to require a higher power source; however, this does not hinder the FM improvement seen in the TE2B case. From this result it is apparent the important role that the tip shape has in drone rotors performances. For high root pitch angles, and consequently high thrust production, the decay for the TE2B rotor performance is less evident than for SB, and this is reflected on a higher FM.

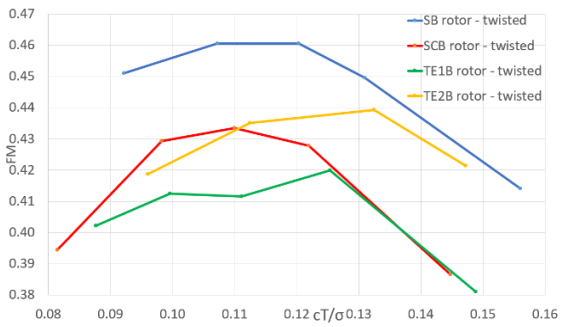

Figure 5.2: FM behavior for twisted blades, in the case of backward curvature

5.3. Twisted blades-backward curvature

A 10 °/m twisting variation is inserted, imposing that the angle at 75% of blade length is equal to the five pitch angles defined in the untwisted case, because in this way the thrust production is the same, according to the BET [14]. This is found to be reasonably true also in the case of small scale rotors, since for all the four rotors the differences between the thrust produced in the untwisted and twisted case are below 5%. Considering the SB rotor, the twisting insertion is shown to improve both the thrust production and the FM, which increases between 5% and 10% in the range studied (see figure 5.2). Considering the curved blade rotors, the improvement is found to be always around 3%. This fact leads to the better behavior of the SB rotor with respect to the TE2B rotor also at high thrust coefficients.

5.4. Untwisted blades-forward curvature

The SCF rotor is compared with the SB. At the tip, a thicker part facing the airflow direction is present, and is responsible of a great drag increasing without bringing any benefit on the thrust production. Moreover, it seems to facilitate the separation of the flow, thus increasing the blade tip vortices dimensions. The flow separation is increased as the root pitch angle increases, and this is reflected on a performance decay for the SCF rotor at high c_T/σ values, while the FM is almost constant up to $c_T/\sigma \approx 0.125$, as depicted in figure 5.4. The vortices developed at the blade tip are shown in figure 5.2, plotting the region of a constant swirling strength equal to 0.01.

The TE1F rotor presents similar characteristics to

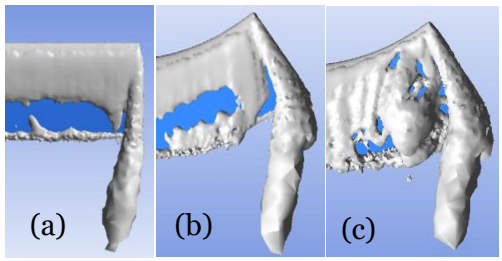

Figure 5.3: Comparison between the contour of the region at constant swirling strength for the SB rotor(a) and the SCF rotor at 19° (b) and 25° (c) of root pitch angle

the SCF, with the area facing the air flow at the tip that is even greater, thus causing a higher drag production and vortex generation. The SCF rotor produces higher thrust than the TE1F at the same root pitch angle, the difference being always between 5% and 9%. A clear improvement is observed when analyzing the TE2F rotor. In fact, TE2F produces around 15% more thrust than the TE1F, and the vortex region at the tip is smaller, so that this loss source is reduced. In fact, TE2F has the best FM between the curved blades for low and medium thrust production, while for high thrust production SCF results as the best configuration.

Comparing the SCB and SCF rotors a similar thrust production is noticed, with differences below 2%, but the SCB rotor presents a 10% less power consumption, this leading to higher FM values.

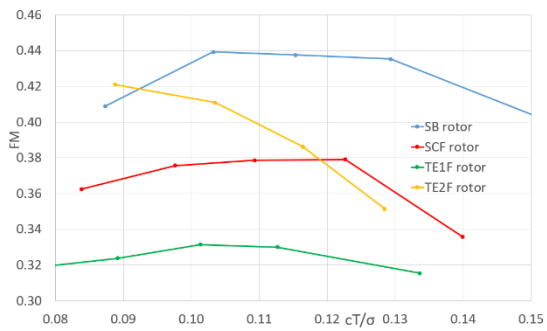

Figure 5.4: FM behavior for untwisted blades in case of forward curvature

The comparison between TE2B and TE2F shows as incrementing the pitch angle there is an increase in the gap between the two cases, with the TE2B rotor behaving better (see figure 5.5).

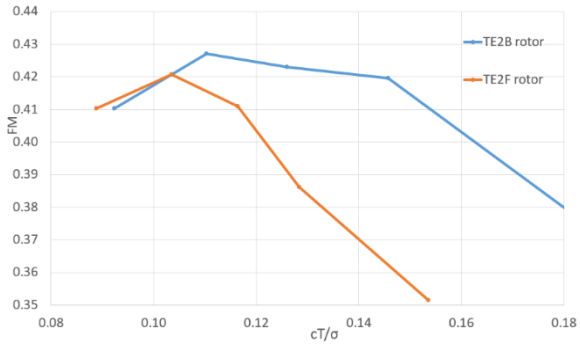

Figure 5.5: Comparison between the TE2B and TE2F rotors

5.5. Twisted blades-forward curvature

The twisting of the forward curved blades is inserted in the same way as previously. The SCF presents an FM improvement between 3% and 11%, while the thrust production is almost similar, with the maximum discrepancy equal to 3%. In the case of TE1F rotor, inserting the twist brings an improvement between 3% and 8 % in the FM, while for the TE2F rotor the benefit is reduced to 2%. From figure 5.6 is apparent how the TE2F rotor is the best configuration in the case of forward curvature, even though the results are lower than in the case of backward curvature.

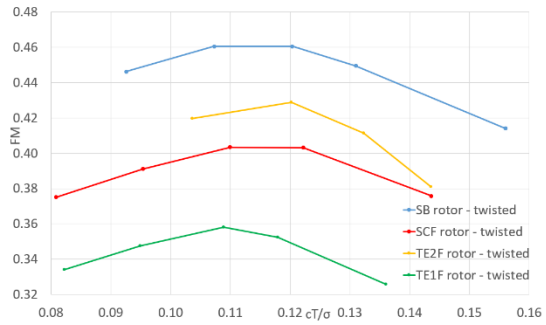

Figure 5.6: FM behavior for twisted blades, in the case of forward curvature

5.6. Axial flight results

Five twisted configurations with a root pitch angle of 26.5° are studied in the case of ascending flight, namely the SB, SCB, TE2B, SCF and TE2F rotors. This flight condition is obtained by imposing a velocity inlet equal to the ascending velocity v_c and keeping the moving domain in rotation with the desired angular speed. At first, the rotational speed is kept constant at 3000 RPM, while the ascending velocity is increased. Then, a different analysis is made by keeping constant the thrust to the value produced in hovering as the climbing velocity increases, by changing the rotational speed. The results of the first analysis respect what predicted in [14], in the sense that the thrust production decrease moving towards higher ascending velocities (see figure 5.7). This can be justified by the fact that the angle of attack α is reduced as v_c

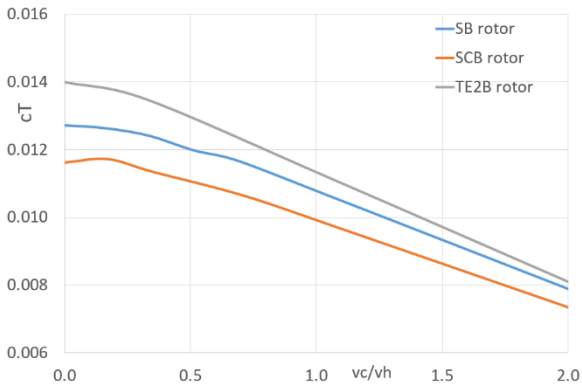

Figure 5.7: Thrust coefficient versus climbing ratio

reaches higher values. For the second analysis, the maximum difference acceptable between the thrust produced in hovering and in the case of axial flight is 2.5%. To understand how the power requirements change with the ascending velocity, the equation 5.1 is plotted:

$$\frac{P_{climb}}{P_h} = \frac{P_{CFD,c} + Tv_c}{P_{CFD,h}} \tag{5.1}$$

In this equation, $P_{CFD,c}$ is the power requirement calculated with the CFD simulations in case of axial flight, which consider the viscous and the induced drag at the rotor disk, without taking into account the power required for the ascending flight, that is added through the parameter Tv_c. $P_{CFD,h}$ is the power required to hover. Every rotor shows an increase in the power requirement with the climbing velocity, with the SB rotor presenting the higher decrease with respect to the hovering case. This behavior is shown in figure 5.7.

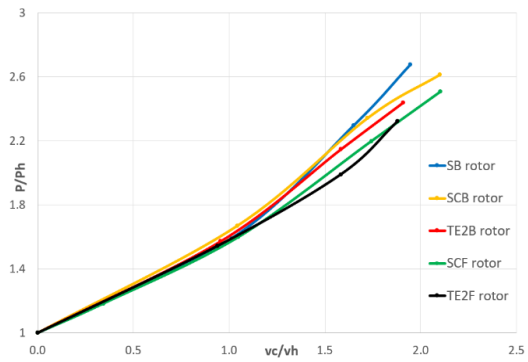

Figure 5.8: Climbing power ratio plotted versus the climbing ratio

A modified FM is defined to compare the rotor performances at different climbing velocities, defined by the ratio between the ideal power required for climbing flight and the real power required for the climbing flight. Each rotor presents a similar behavior, with FM_{climb} that is almost constant or is increasing for low climbing velocities, while for higher climbing velocities, the decrement is evident, see figure 5.9.

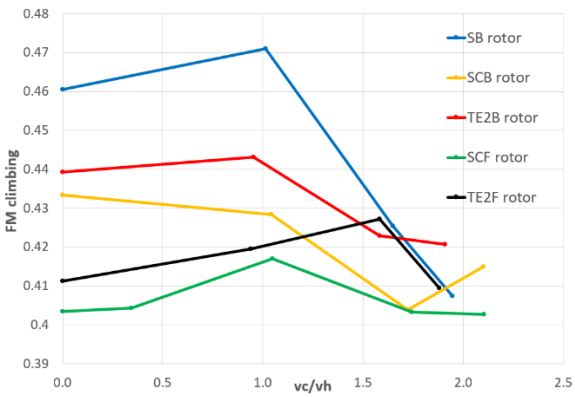

Figure 5.9: FM_{climb} plotted versus the climbing ratio

5.7. Tip modification results

The three rotors SB3, TE3B and TE3F are analyzed in hovering condition to check the impact of the tip shape on rotor performances. Comparing SB and SB3, it is noticeable how the tip modification brings a reduction in the thrust produced, always between 5% and 8.8% , while the FM presents variations between 0.53% and 1.57%. From the graph 5.10 it can be said that up to values of $c_T/\sigma \approx 0.115$, the SB3 rotor behaves better than the SB, requiring less power to hover for the production of the same thrust amount.

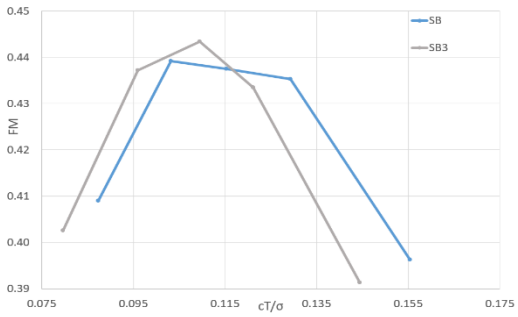

Figure 5.10: Comparison between SB and SB3 rotors in hovering condition

Also in the case of backward curvature, the tip modification brings reduction in the thrust between 7% and 15% when compared with TE2B rotor, while the FM is similar. Up to values of $c_T/\sigma \approx 0.135$ the TE3B rotor is preferable, but at high thrust values (which correspond to high root pitch angles), the TE3B rotor presents a strong performance decay, which makes the TE2B rotor operate better. In the case of forward curvature, the comparison between TE1F, TE2F and TE3F rotors brings interesting results, shown in figure 5.11. In fact, even though the thrust production is around 2% less than TE2F case for the root pitch angles tested, the FM improvement is very high, between 4.3% and 9.3%, so that the TE3F rotor results to be the best configuration for a great interval of thrust values. Comparing the tip modified rotors SB3, TE3B and TE3F a better insight in the effect of inserting a curvature can be made, since the tip presents the same shape. Considering rotor with the same root pitch angle, inserting a curvature increase the thrust produced, and this is verified for all the five angles tested. At

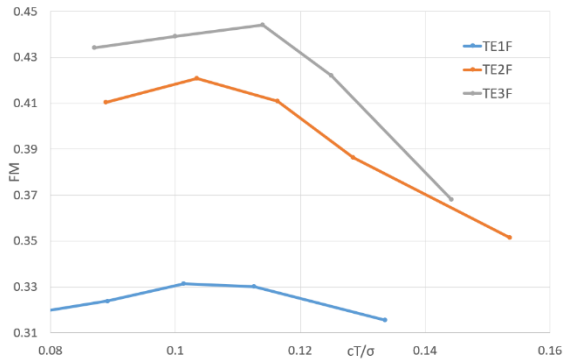

Figure 5.11: Comparison between TE1F, TE2F and TE3F rotors in hovering conditions.

low thrust production, the FM of SB3 and TE3F rotors is similar, while TE3B rotor appear to be less efficient. When moving towards higher thrusts, the TE3B rotor shows a less evident decay, so its use is preferable in those cases. These discussions are showed in figure 5.12.

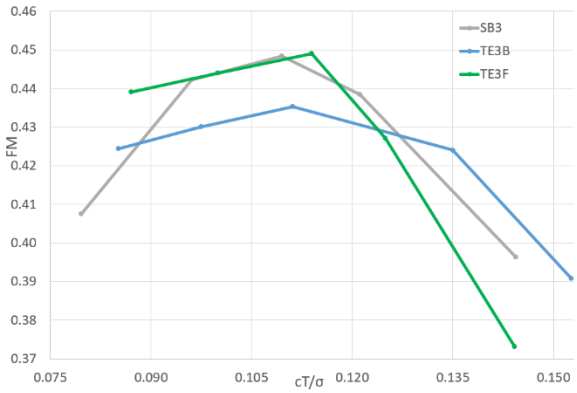

Figure 5.12: Comparison between SB3, TE3B and TE3F rotors in hovering conditions

5.8. Comparison between CFD and experimental results

The SB, SCB, TE1B and TE2B rotors in an untwisted configurations with a root pitch angle of 15°, and in a twisted configurations with a root pitch angle of 22.5° are experimentally tested using the test bench developed by Ines for a IST University project, which characteristics are presented in [20]. The first experimental test is realized with the SB untwisted rotor, which is put in rotation at different speeds, between 1990 RPM and 5043 RPM to detect the variation of thrust production and power requirement. The comparison with CFD simulations, presented in figures 5.13-5.14, shows good accordance between experimental and CFD results. The thrust measured is always higher than the one computationally predicted, and this could be due to the flexibility of the blades, that could generate an actual angle of attack different from the one used for the CFD simulations. The FM presents similar values, with differences that are below the 5%, see figure 5.15. The second experimental test campaign is realized by putting in rotation the rotors at 3000 RPM, and registering the thrust produced as well as the power requested to permit the motion. The measured thrust appears to be always higher than the one predicted by CFD, with a maximum

discrepancy of 16% in the case of the SCB twisted rotor, except for the TE1B untwisted rotor. This fact is addressed to be caused by the flexibility of the

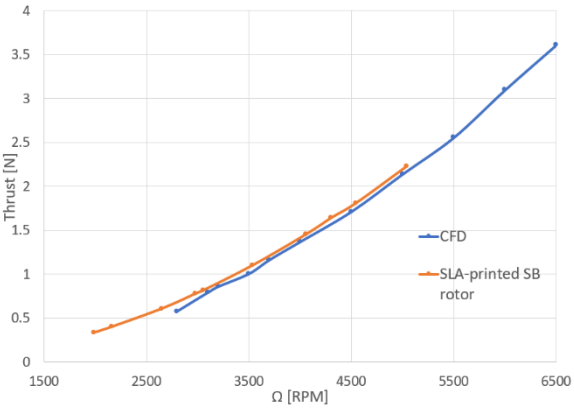

Figure 5.13: Thrust behavior vs rotational speed, obtained by CFD simulations and experimental tests

SLA-printed blades, which may cause the rotor to operate at higher α. One other cause could derive from the choice of the moving domain dimensions, which appear to strongly influence the results in term of thrust produced as already stated [13]. However, when looking at the FM results, the discrepancy is always below 4% for SB, SCB and TE1B rotors. When studying the TE2B rotor, the experimental results state a FM 8% higher than what predicted by CFD. It seems that the TE2B configurations present the highest performances between the rotors studied, at 3000 RPM. The results are presented in table 4.

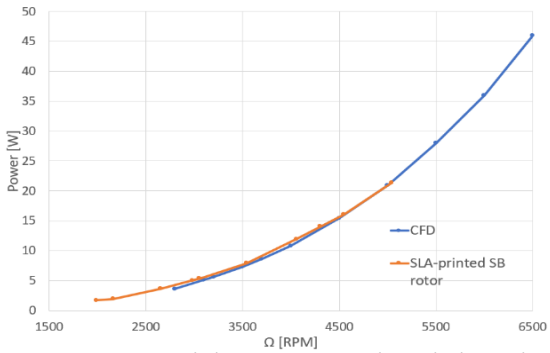

Figure 5.14: Power behavior vs rotational speed, obtained by CFD simulations and experimental tests

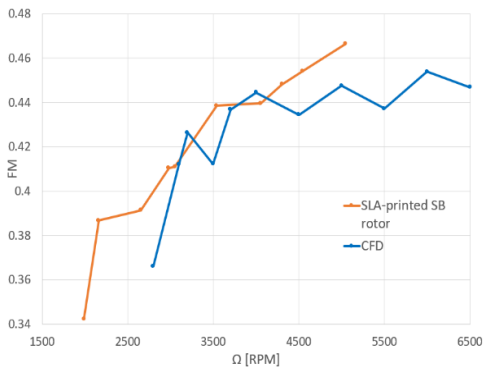

Figure 5.15: FM at various rotational speed, CFD vs experiment

Table 4: Comparison between CFD and experimental results at 3000 RPM

Rotor	Experimental Thrust	CFD thrust	ΔThrust	Experimental FM	CFD FM	Δ FM
SB 15°	0.786 N	0.738 N	6.5%	0.410	0.409	0.4%
SB twisted 22.5°	0.849 N	0.779 N	9%	0.434	0.451	3.8%
SCB 15°	0.695 N	0.696 N	0.16%	0.385	0.393	1.95%
SCB twisted 22.5°	0.802 N	0.688 N	16.55%	0.387	0.394	1.82%
TE1B 15°	0.702 N	0.737 N	4.8%	0.387	0.397	2.47%
TE1B 22.5°	0.767 N	0. 741 N	3.47%	0.414	0.402	2.84%
TE2B 15°	0.849 N	0.780 N	8.78%	0.444	0.410	8.26%
TE2B 22.5°	0.853 N	0.812 N	5.08%	0.455	0.419	8.62%

6. 3D printing

6.1. FDM printing results

Four different printing methodologies are tested, choosing an extra fine thickness of 0.06 for the extruded material to enhance the surface quality. In method 1 the rotor plane is set parallel to the building plate, with the support material attached to the blade intradox, while in method 2 the rotor plane is orthogonal to the building plate, so that the support is made by a thin wall. In these two cases, the support material is in PLA, as the printed part. Method 1 resulted in the presence of some defects in the intradox, due to the presence of the support. The surface quality of the second method is higher, even though the vibration of the building plate caused the airfoil shape to be distorced. These considerations led to the definition of method 3, in which the rotor is cut in two parts, so that is possible to always impose the contact between the leading edge and the support material. For this method, the support material is produced in PVA. After the sandpapering and the application of a plastic wax, the results of method 3 are a good surface quality and a good representation of both leading and trailing edge. The fourth method is realized printing the blade standing. This method has proven to improve the surface quality, but the vibrational effects causes some inaccuracies in the tip representation. In conclusion, method 3 seems the best for the 3D printing of this blade geometry. In term of production time, a 2-bladed rotor could be printed in about 13 hours.

6.2. SLA printing results

The Prusa SL1 machine is used for the tests. Due to its dimensions, each rotor is cut in two parts. The SB, SCB TE1B and TE2B rotors are printed, both untwisted with a root pitch angle of 15° and twisted with the root pitch angle of 22.5°.
A layer height of 0.05 mm is chosen for the and the post processing curing is realized with the machine Prusa CW1, which permits a curing in about 10 minutes. The results are very good in term of surface quality, which is higher than the FDM printed parts. Another positive aspect of the SLA technique is the printing time, since in a single session up to 8 blades could be printed. The printing time for a single session is about 6 hours. The surfaces in contact with the support material are not flat, so that the sandpapering with a fine 1000-grit paper is needed.

These aspects made difficult the alignment between the rotor and the rotational axis for the experimental tests.

7. Conclusions

BEMT theories are not applicable for the study of small-scale propeller, because they do not take into account the complex 3D flows which characterize the low Re regime. The MRF method was used for the simulation of hovering and axial flight of different rotors. The results showed a good improvement in the performance when using the tip shape 3, in particular with the TE3F rotor for low pitch angle and the TE3B rotor for high pitch angles. The TE2B rotor appeared to behave better than the straight SB rotor at high pitch angles, for which it is preferred. Both the FDM and SLA techniques have been tested for the production of rotors. The SLA-printed blades have been tested in hovering conditions. The results from such analyses are in good accordance with the CFD results. From the experimental data, the TE2B rotor has interesting performances, both in the untwisted and twisted configuration. An improvement in CFD results can be reached by fitting the proper moving domain dimension for the study of that case, by comparison with the experimental data.

Bibliography

[1] R. D'Andrea, «Guest editorial can drones deliver?» *IEEE trasanctions on automatic science and engineering,* vol. 11, n. 3, pp. 647-648, 2014.

[2] A. Goodchild e J. Toy, «Deliver by drone: an evaluation of unmanned aerial vehicle technology in reducing CO2 emissions in the delivery service industry» *Transport. Res. Part D Transport and Environment,* 2017.

[3] «Volocopter GmbH» [Online]. Available: https://www.volocopter.com/en/product/. [Last visit 04 05 2020].

[4] «Airbus» Airbus S.A.S., [Online]. Available: https://www.airbus.com/innovation/urban-air-mobility/vehicle-demonstrators/vahana.html. [Last visit 04 05 2020].

[5] E. V. Laitone, «Wind tunnel testing of wings at Reynolds number below 70000» *Experiments in fluids,* n. 23, pp. 405-409, 1997.

[6] F. W. Schmitz, «Aerodynamik des flugmodells», Berlin-Charlottenburg: C. Lange, 1942.

[7] Ohtake, Tomohisa, Nakae, Yusuke, Motohasi e Tatsuo, «Nonlinearity of the aerodynamic characteristics of NACA0012 aerofoil at low Reynolds numbers» *Journal of the Japan society for aeronautical and space sciences,* vol. 55, n. 644, pp. 439-445, 2007.

[8] C. Pranesh, M. Sivapragasam, M. D. Deshpande e H. K. Narahari, «Negative lift characteristics of NACA 0012 aerofoil at low Reynolds numbers» *Sadhana,* vol. 44, n. 1, 2019.

[9] K. Yonemoto, K. Takato, H. Ochi e S. Fujie, «Kutta condition violation in two-dimensional NACA0012 airfoil at low Reynolds number» *26th AIAA Applied Aerodynamics Conference,* p. 6399, 2008.

[10] M. Ramasamy, «Flowfield of a rotating-wing micro air vehicle» *Journal of Aircraft,* vol. 44, n. 4, pp. 1236-1244, July 2007.

[11] M. Benedict, J. Winslow, Z. Hasnain and I. Chopra, «Experimental investigation of micro air vehicle scale helicopter rotor in hover» *International Journal of Micro Air Vehicles,* vol. 7, no. 3, pp. 231-255, 2015.

[12] H. A. Kutty and P. Rajendran, «3D CFD simulation and experimental validation of small APC slow flyer propeller blade» *Aerospace ,* vol. 4, no. 1, 25 February 2017.

[13] M. Stajuda, M. Karczewski, D. Obidowski and K. Jozwik, «Development of a CFD model for propeller simulation» *Mechanics and Mechanical engineering,* vol. 20, no. 4, pp. 579-593, 2016.

[14] J. G. Leishman, «Principles of helicopter aerodynamics», II edition, Cambridge Press, 2006.

[15] M. Drela, «XFOIL: an analysis and design system for low Reynolds numbers airfoils» *Low Reynolds number aerodynamics,* pp. 1-12, 1989.

[16] C. Young, «The prediction of helicopter rotor hover performance using a prescribed wake analysis«, London: Her Majesty's Stationery Office, 1976.

[17] R. Marpu, R. Sankar, T. Norman, T. Egolf e S. Makinen, «Analysis of the UH-60A Rotor Loads Using Wind Tunnel Data» *51st AIAA Aerospace Sciences Meeting,* n. 0635, p. 635, 2013.

[18] Ansys Inc., «Ansys Fluent user's guide», version 18.1, 2017.

[19] Ansys Inc., «Ansys Fluent theory guide», version 18.1, 2017.

[20] I. S. Amado, «Experimental comparison of planar and coaxial rotor configurations in multi-rotors», Master thesis, IST Lisboa, 2017.